Macromolecules
ARTICLE

Macromolecules **2010**, *43*, 2357–2363 **2357**
DOI: 10.1021/ma902862u

Enhanced Mechanical Properties of Graphene-Based Poly(vinyl alcohol) Composites

Xin Zhao, Qinghua Zhang,* and Dajun Chen

State Key Laboratory for Modification of Chemical Fibers and Polymer Materials, College of Materials Science and Engineering, Donghua University, Shanghai 201620, P. R. China

Ping Lu

Center of Analysis and Measurement, Donghua University, Shanghai 201620, P. R. China

Received December 30, 2009; Revised Manuscript Received January 30, 2010

ABSTRACT: Graphene, flat carbon nanosheets, has generated huge activity in many areas of science and engineering due to its unprecedented physical and chemical properties. With the development of wide-scale applicability including facile synthesis and high yield, this exciting material is ready for its practical application in the preparation of polymer nanocomposites. Here we report that nanocomposites based on fully exfoliated graphene nanosheets and poly(vinyl alcohol) (PVA) are prepared via a facial aqueous solution. A significant enhancement of mechanical properties of the graphene/PVA composites is obtained at low graphene loading; that is, a 150% improvement of tensile strength and a nearly 10 times increase of Young's modulus are achieved at a graphene loading of 1.8 vol %. The comparison between the experimental results and theoretical simulation for Young's modulus indicates that the graphene nanosheets in polymer matrix are mostly dispersed randomly in the nanocomposite films.

1. Introduction

Graphene, a two-dimensional material, is composed of several planar sheets of sp^2-bonded carbon atoms. Since experimentally discovered in 2004,[1] graphene with unique properties has become one of the most exciting materials today. Theoretical and experimental results on individual graphene nanosheets exhibit extremely high values of Young's modulus (~1000 GPa), fracture strength (~125 GPa),[2] elastic modulus (~0.25 TPa),[3] thermal conductivity (~5000 W m^{-1} K^{-1}),[4] mobility of charge carriers (~200 000 cm^2 V^{-1} s^{-1}),[5] specific surface area (calculated value, ~2630 m^2 g^{-1}),[6] and fascinating transport phenomena such as the quantum Hall effect.[7] These properties make graphene very promising for many applications such as solar cells and hydrogen storage,[8] sensors,[9] batteries,[10] supercapacitors,[5,11] and nanocomposites.[12,13]

At present, nanocomposites employing carbon-based reinforcement materials are dominated by carbon nanotubes (CNTs). However, the development of CNT-reinforced composites has been impeded by their difficult dispersion in matrix and their higher costs. In our pervious work, a new spraying method was used to uniformly disperse SWNT in a polymer matrix, and SWNT-based nanocomposites with high performance were obtained.[14] Compared to carbon nanotubes, graphenes continue to attract considerable attention because of their outstanding mechanical and electrical properties as well as high aspect ratio and low density, which results in one of the ideal candidates for developing functional and structural graphene-reinforced composites. Incorporation of graphene into ceramics[15,16] or polymer matrices[17] remarkably improves the properties of the materials. Wakabayashi et al.[18] employed a solid-state shear pulverization (SSSP) to produce polypropylene−graphite nanocomposites, revealing a 100% increase in Young's modulus and a ~60% increase in yield strength as a function of the addition of 2.5 wt % graphite. Liang et al.[19] prepared a nanocomposite of graphene/polymer with a 76% increase in tensile strength and a 62% improvement of Young's modulus at a loading of 0.7 vol % graphite oxide. Wang et al.[20] reported that a freestanding and flexible graphene/polyaniline composite paper gave a favorable tensile strength of 12.6 MPa. Therefore, more attention has been drawn to graphene as a potential reinforcement material in the next generation of composite materials. Meanwhile, the electrically conductive property can be obviously improved via adding the nanosheets into a matrix. Graphene nanosheet-based polystyrene composites synthesized by a liquid-phase blend route exhibited extraordinarily low electrical percolation threshold of 0.1 vol %.[21] Composite films of noncovalent functionalized graphene sheets/sulfonated polyaniline revealed improved conductivity of 0.2 S cm^{-1}, good electrocatalytic activity, and stability, reported by Bai et al.[22]

One of the key points to the successful development of graphene-based nanocomposites and to the improvement of their performance is the dispersion of nanofillers in a polymer matrix. Because of their high specific surface area, graphene tends to form irreversible agglomerates or even restack due to van der Waals interactions. Full utilization of graphene nanosheets in polymer nanocomposite application will inevitably depend on their abilities to achieve full exfoliation and complete dispersion in the polymer matrix. To successfully achieve the reinforcing potential of graphene nanolayers, they must be fully exfoliated in process of preparation. Under suitable conditions, graphite oxide can undergo exfoliation completely in water, yielding colloidal suspensions of almost entirely individual graphene oxide nanosheets.[23] Such nanosheets can be chemically functionalized, dispersed in polymer matrices, and deoxygenated to yield novel composites. Exfoliated graphene oxide nanosheets can be reduced using hydrazine hydrate, resulting in their reaggregation and

*Corresponding author: e-mail qhzhang@dhu.edu.cn; Fax 0086 21 67792854.

Published on Web 02/09/2010

subsequent formation of a high-surface-area carbon material which consisted of thin graphene-based sheets.[24] Li et al.[25] reported that chemically converted graphene nanosheets obtained from graphite readily form stable aqueous colloids through electrostatic stabilization and consequently developed a facile approach to large-scale production of aqueous graphene dispersion without the need for polymeric or surfactant stabilizers. Moreover, the good dispersion of these nanosheets in the polymer matrix is an important aspect to exhibit good interfacial strength with the matrix. Stankovich et al.[26] treated graphene oxide with organic isocyanates, and these isocyanate-treated graphene oxides were then exfoliated into functionalized graphene oxide nanoplatelets, exhibiting a stable dispersion in polar aprotic solvents. So molecular-level dispersion of individual, chemically modified graphene sheets within polymer hosts could be formed.[27] This group[28] also reported a stable aqueous dispersion of graphitic nanoplatelets by coating reduced graphene oxide nanoplatelets with an amphiphilic polymer, so that it improved the ability to achieve good dispersion of the nanofiller component in the polymer matrix of choice.

Recently, we prepared graphene-reinforced poly(vinyl alcohol) (PVA) composite films by incorporating graphene oxide into PVA aqueous solution and then reduced graphene oxide to graphene nanosheets. To full exfoliate the nanofillers, graphite was oxidized with $KMnO_4$ in concentrated H_2SO_4 and then reduced with hydrazine, and sodium dodecylbenzenesulfonate (SDBS) was used to stabilize the aqueous dispersion of graphene nanosheets. The obtained composites of PVA and graphene exhibited a significant enhancement of mechanical property at a low loading of graphene.

2. Experimental Section

2.1. Materials. Graphite with an average particle size of 30 μm and a purity of >99% were supplied from Shanghai Yifan Graphite Co., Ltd. Concentrated sulfuric acid (H_2SO_4) and hydrochloric acid (HCl) were purchased from Pinghu Chemicals, China. Potassium permanganate ($KMnO_4$) was purchased from Reagent No. 1 Factory of Shanghai Chemical Reagent Co., Ltd. Sodium nitrate ($NaNO_3$) was purchased from Shanghai Kechuang Chemicals Co., Ltd. Hydrazine hydrate (85%) and SDBS were purchased from Sinopharm Chemical Reagent Co., Ltd. Hydrogen peroxide (H_2O_2) was purchased from Shanghai Jinlu Chemical Co., Ltd. Poly(vinyl alcohol) (PVA) with $M_w \approx$ 100 000 was obtained from Anhui Wanwei Updated High-Tech Material Industry Co., Ltd. The materials were directly used without further purification.

2.2. Preparation of Graphite Oxide and Graphene Nanosheets. Graphite oxide, a pseudo-two-dimensional solid in bulk form, was prepared from natural graphite powder by oxidation with $KMnO_4$ in concentrated H_2SO_4 according to Hummers' method.[29] Concentrated H_2SO_4 (46 mL) was poured into the 250 mL three-neck flask and stirred in an ice bath until the temperature dropped to 0−3 °C. Natural graphite (2 g) and $NaNO_3$ (1 g) were added and stirred uniformly. $KMnO_4$ (30 g) was gradually added with stirring and cooling in order to keep the temperature below 20 °C. The solution was heated to 35 ± 3 °C and maintained for 30 min. Then, distilled water was slowly added, and the temperature was controlled lower than 100 °C. After 15 min, this reaction was terminated by addition of a large amount of distilled water and 30% H_2O_2 solution (5 mL). The mixture was filtered and washed with 5% HCl aqueous solution and water. The sample of graphite oxide was obtained after drying. To prepare graphene nanosheets, 100 mg graphite oxide was dispersed in 100 mL of water to create a yellow-brown dispersion, and the exfoliation of graphite oxide to graphene oxide was achieved by sonication with a cylindrical tip for 30 min. Then the resulting homogeneous solution was mixed with 80 μL of hydrazine solution as a reducing agent, and 350 μL of ammonia solution was added to adjust pH to around 10. After stirred for a few minutes, the mixed solution was heated at ~95 °C for 1 h. The reduced product was isolated by filtration through polytetrafluoroethylene (PTFE) membrane (0.22 μm), washed with water and methanol, and dried for 24 h in vacuum oven. Then graphene nanosheets, that is, the reduced graphene oxide, were obtained.

2.3. Preparation of Graphene/PVA Composites. To prepare the composites, graphene oxide (GO)/PVA composites were first prepared, and the process of reduction from GO to graphene followed. The dispersion of exfoliated GO (1 mg/mL) was prepared in 0.5 wt % SDBS solution by sonication. For composite fabrication, certain PVA powder was blended with this exfoliated GO solution (10 mL) described above and stirred at 85 °C for ~6 h. This resulting homogeneous dispersion was mixed with 8 μL of hydrazine solution and 35 μL of ammonia solution (28%), and after being stirred for ~30 min, the mixed solution was put in a oil bath at ~95 °C for 1 h. The dispersion was cast onto clean glass plates using a doctor blade and dried at 60 °C for ~24 h in an oven for film formation. The composites containing 0.5, 1, 3, and 5 wt % graphene nanosheets and a parallel sample of pure PVA with the same amount of SDBS were prepared. As a matter of convenience, the filler concentration was transformed from mass fraction w (wt %) to volume fraction v (vol %) by the following equation:

$$v = \frac{w\rho_p}{w\rho_p + (1-w)\rho_g}$$

Here, v and w are the volume fraction and mass fraction of graphene nanosheets. ρ_p and ρ_g represent the density of PVA matrix and graphene nanosheets, which can be taken as 1.3 g/cm^3 [27] and 2.2 g/cm^3, respectively. Then, the volume fractions of graphene nanosheets filled into the PVA matrix can be obtained as 0.3, 0.6, 1.8, and 3.0 vol %.

2.4. Characterization. The UV−vis absorption spectra were measured on a Lambda 35 (Perkin-Elmer) spectrophotometer. Raman spectra were recorded using a LabRam-1B Ramen spectroscope, with He−Ne laser excitation at 632.8 nm, scanning for 50 s. X-ray diffraction (XRD) measurements were carried out using a Rigaku D-max-2550 diffractometer with Cu Kα radiation. In order to avoid the influence of the thickness of specimens, all the samples with a same thickness of 20 μm were prepared for the measurements. Transmission electron microscopy (TEM) was performed with a Hitachi H-800 electron microscope operating at an accelerating voltage of 100 kV. Typical tapping-mode atomic force microscopy (AFM) measurements were taken using Multimode SPM from Digital Instruments with a Nanoscope IV controller made by Veeco Instruments Inc. Samples for AFM images were prepared by depositing a dispersed graphene solution (0.1 mg mL^{-1}) onto a freshly cleaved mica surface and allowing them to dry in air. The fracture surface morphology of the composite was observed on a HITACHI S-4800 at an accelerating voltage of 3.0 kV. The sample was fractured in liquid nitrogen and gold-sputtered prior to observation. For measurement of the mechanical properties of the composites, the sample were cut to sheets with a width of 10 mm, and the measurement was conducted with an XQ-1 instrument made in China. The lower grip was fixed and the upper grip rose at a rate of 5 mm/min. The gauge length was 20 mm.

3. Results and Discussion

3.1. Exfoliation of Graphene. In the process of reduction, the yellow-brown color characteristic of the graphite oxide dispersion changed into black following reduction, suggesting that deoxygenation of the graphite oxide nanosheets had effectively come about. As shown in Figure 1, UV−vis spectra

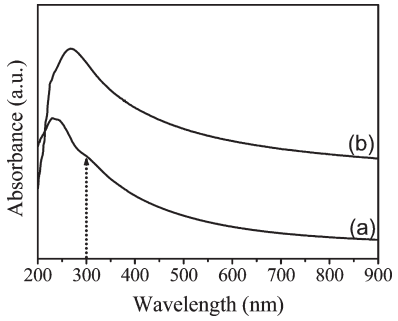

Figure 1. UV−vis spectra of aqueous dispersion of 0.1 mg/mL: (a) graphite oxide and (b) graphene.

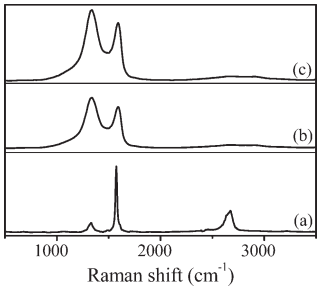

Figure 2. Raman spectra of (a) pristine graphite, (b) graphite oxide, and (c) graphene.

of the samples confirm the transition of graphite oxide into graphene. The curve of graphite oxide dispersion exhibits a maximum at 231 nm and a tiny shoulder at ~300 nm, which are respectively attributed to $\pi \rightarrow \pi^*$ transitions of aromatic C−C bonds and $n \rightarrow \pi^*$ transitions of C=O bonds. Whereas, for the reduced form, the absorption peak of the graphene dispersion at 231 nm red-shifts to ~270 nm, and a significant increase in absorbance in the whole spectral region (> 231 nm) is noticed. These effects suggest that the electronic conjugation within the carbon framework of the graphene nanosheets has been restored upon hydrazine reduction, which is in agreement with the previous reports.[24,25,30]

Raman spectroscopy is employed to evaluate the transform from pristine graphite to graphite oxide and then to graphene. As shown in Figure 2a, the first-order Raman spectra of pristine graphite contain a strong band at ~1581 cm^{-1} (G band) and a very weak band at ~1340 cm^{-1} (D band). The G band and D band are attributed to the first-order scattering of the E_{2g} vibrational mode in graphite sheets[31] and structural defects (disorder-induced modes), respectively. The second-order spectra are inspected as 2D band at 2680 cm^{-1} which is the overtone (second harmonic) of the D band. The 2D bands of graphite oxide and graphene are seen to broaden and decrease in relative intensity, indicating presence of defects in graphitic materials.[32] The D band and G band are also observed for graphite oxide and graphene, as shown in Figure 2b,c, although the D band at 1573 cm^{-1} becomes prominent and the ratios of D- to G-band intensity (I_D/I_G) increase from 0.14 for pristine graphite to 1.23 and 1.57 for graphite oxide and graphene, respectively. According to the previous work which indicated that I_D/I_G could be used to qualitatively characterize the change of defects in the carbon nanotubes,[33,34] I_D/I_G should decrease in the process of reduction. However, I_D/I_G of graphene is higher than that of graphite oxide. Stankovich et al.[24] interpreted the increase I_D/I_G from graphite oxide to graphene by assuming that reduced state increases the number of aromatic domains of smaller overall size in graphene, leading to an enhancement

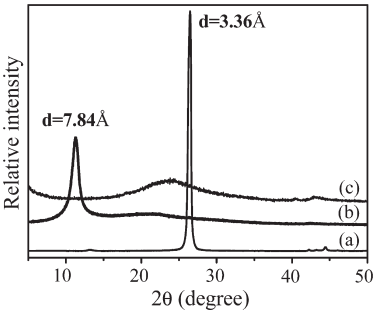

Figure 3. XRD pattern of (a) pristine graphite, (b) graphite oxide, and (c) graphene. The interlayer distance is represented by *d*.

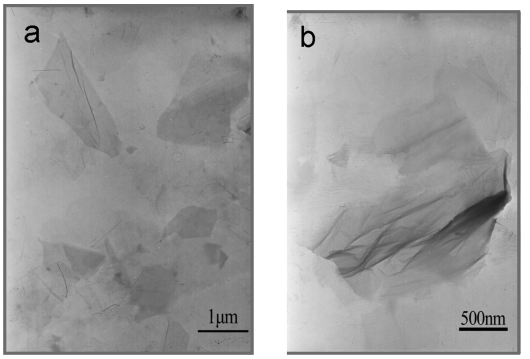

Figure 4. TEM images of graphene nanosheets with different magnification.

of the I_D/I_G ratio. While Paredes et al.[35] solved this apparent contradiction, attributing to the fact that the carbon lattice in graphite oxide has developed some degree of amorphous character due to oxidation process itself, they noted that the distortion of the 6-fold rings was removed during the reduction process, and the carbon lattice returns to an essentially graphitic, but highly defected, state.

X-ray diffraction determines the changes of interlayer distance in nanosheets shown in Figure 3. The diffraction peak in the XRD pattern of graphite oxide appeared to be 11.3°, corresponding to the layer-to-layer distance of ~0.78 nm. It is significantly larger than that of pristine graphite (~0.34 nm), due to the intercalating oxide functional groups.[36] Whereas the XRD pattern of graphene shows a typical broad trace with an obvious disappearance of the characteristic peaks, it can be explained that graphene was exfoliated into a monolayer or few-layers, resulting a new lattice structure, which is significantly different from the pristine graphite.[37]

TEM images of the nanosheets are shown in Figure 4. Apparently, the fully exfoliated graphenes are observed with the average size of nanosheets of 1−2 μm. Some graphene nanosheets crumple due to thin thickness, shown in Figure 4b. Atomic force microscopy (AFM) is used to determine the thickness of the graphene-based sheets. Figure 5 displays a typical tapping-mode AFM image of graphene nanosheets deposited onto a mica substrate from an aqueous dispersion, exhibiting the sheets heights of ~0.8 nm. The fact reveals characteristic of a fully exfoliated graphene nanosheet.[35]

3.2. Morphology and Structure of Nanocomposites. The quality of nanofiller dispersion in the polymer matrix directly correlates with its effectiveness for improving mechanical, electrical, impermeability, and other properties. The properties of a composite are also intimately linked to the aspect ratio

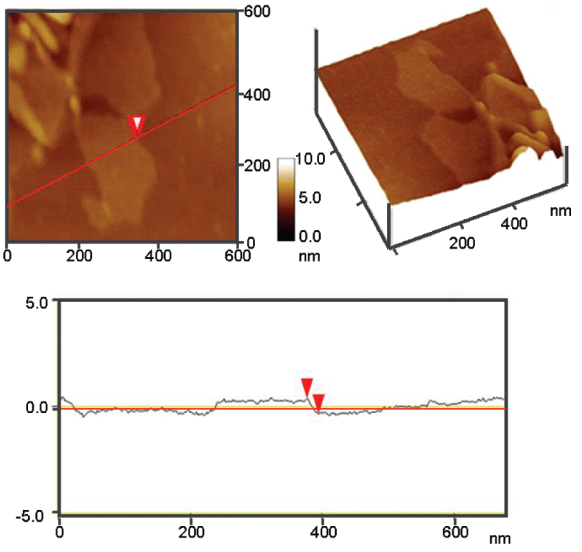

Figure 5. A typical AFM tapping-mode image of graphene nanosheets deposited onto a mica substrate from an aqueous dispersion with superimposed cross-section measurements taken along the red line, indicating a sheet thickness of ~0.8 nm.

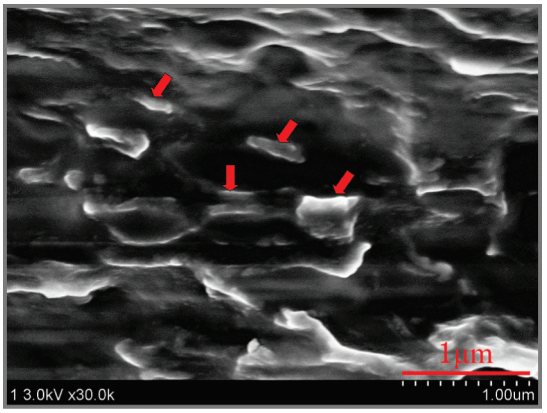

Figure 6. FESEM image of cross section of composite sample with a loading of 1.8 vol % graphene in PVA. The rows point to the graphene nanosheets dispersed in the PVA matrix.

and surface-to-volume ratio of fillers. Of great significance is that the successful formation of graphene dispersions enables the use of conventional low-cost processing techniques to create new graphene-based materials. To well disperse the nanosheets into a polymer, the graphene oxide/PVA nanocomposites were first prepared, and then the process of reduction from GO to graphene followed. The aqueous dispersion of exfoliated GO at the aim of SDBS with sonication were blended with PVA powder. This resulting homogeneous dispersion was mixed with hydrazine solution to reduce the GO nanosheets. The dispersion was cast onto clean glass plates, and the nanocomposites were thus prepared.

Figure 6 shows a FESEM image of the cross-section of the graphene/PVA nanocomposite with a loading of 1.8 vol % graphene nanosheets. The image demonstrates that most of the graphene nanosheets are fully exfoliated and clearly well-dispersed in the PVA matrix, while there are a few restacks together, which might affect the degree of mechanical improvement. The image also reveals that the graphene nanosheets randomly disperse as 3D network through the polymer matrix, while do not just align parallel to the surface of the sample film. This phenomenon is in agreement with

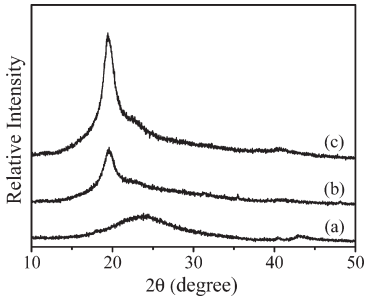

Figure 7. XRD pattern of (a) graphene powder, (b) pure PVA, and (c) graphene/PVA composites with 0.6 vol % loading of graphene.

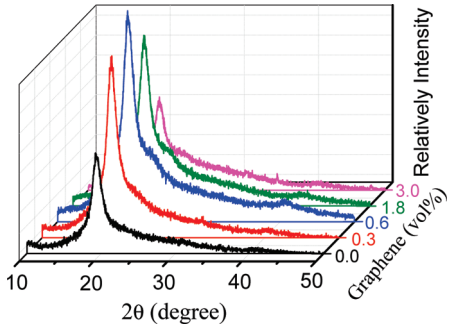

Figure 8. XRD patterns of graphene/PVA composites with various graphene contents.

the theoretical prediction for the mechanical properties of the graphene/PVA nanocomposites in the following discussion.

XRD is an effective method to evaluate the interlayer changes of graphite-related powders and crystalline properties of composite. As shown in the Figure 7, the XRD patterns exhibit a broad peak of graphene and the characteristic peak of PVA at $2\theta = 19.5°$. However, as dispersing the graphene nanosheets into the PVA matrix (curve c), the broad peak in graphene disappears in the composites, suggesting the disorder and loss of structure regularity of the graphene. The same results also can be found in the composites with various graphene loadings, as shown in Figure 8. Thus, the graphene nanosheets are considered to be exfoliated and dispersed at the molecular level into the PVA matrix. To further confirm this point, a parallel sample was prepared, containing 0.6 vol % pristine graphite in PVA. Because of the highly regular structure of graphite, the XRD pattern of the pristine graphite/PVA composites still remains the obvious characteristic peak of graphite at $2\theta = 26.5°$.

PVA is well-known to be a typically semipartially crystalline polymer, existing a strong intensity of XRD at $2\theta = 19.4°$.[38] Figure 8 shows a feeble bulge $2\theta = 40.4°$ and a large part of the intensity of the composites that is the (101) diffraction peak of PVA crystal at $2\theta = 19.4°$. The increase in the intensity of the (101) diffraction corresponds to the increase in the number of PVA chains packing together, resulting in a large size of the crystallite in the PVA sol−gels.[39] As adding the graphene nanosheets into PVA, the intensity of the (101) diffraction rises first and then drops, which means the crystallinity of composites with 0.6 vol % loading of graphene is larger than others. It could be assumed that at a lower loading level the fully exfoliated and well-dispersed graphene nanosheets act as nucleating agents, and thus the crystallinity of the composites is improved. On the other hand, at a high loading level, the nanosheets tend to restack and their surface area ratio reduces;

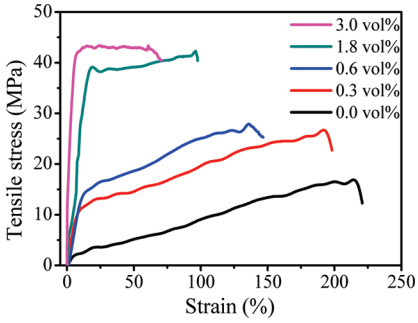

Figure 9. Typical stress−strain plots of the composites with various graphene loadings.

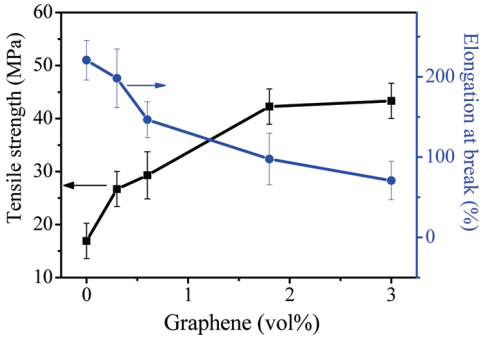

Figure 10. Mechanical properties of graphene/PVA nanocomposites with various graphene loadings: tensile strength (left) and elongation at break (right) versus graphene loadings.

therefore, the further addition of the graphene might hinder the regular arrangements of the PVA chains and lead to the declined crystallinity of the graphene/PVA.

3.3. Mechanical Properties. As described above, the aim of incorporating graphene into the polymer matrix is to improve its mechanical properties and thermal stability. The homogeneity of composites and the stronger interfacial interaction between nanofillers and the polymer matrix should have a significant effect on the mechanical properties. Figure 9 shows the relationship between graphene loading and tensile strength of the composites. It is obvious that the addition of graphene into the polymer matrix has a significant influence on the mechanical behavior. Upon the graphene nanosheet loading, the mechanical behavior of the composites apparently exhibits an enhancing trend. The tensile strength of the composite containing 1.8 vol % graphene is up to 42 MPa, while that of the PVA parallel sample is 17 MPa; i.e., the tensile strength increased by 150%. The increasing trend is especially clear with lower loading. For example, the addition of 0.6 vol % graphene into the matrix causes the increase of modulus increases by 73%. Figure 10 shows that the elongation at break of the composites gradually decreases with graphene loading. The value of the elongation at break decreases to 98% for the composite with 1.8 vol % loading from 220% for parallel sample. The reason may be attributed to a large aspect ratio and the interaction between graphene and the matrix, which restricts the movement of the polymer chains.

On the other hand, as further increasing graphene content from 1.8% to 3.0%, the tensile strength increase slightly from 42 to 43 MPa, without a pronounced change, and there is also a slight influence on the elongation of the composites. Here, it is assumed that as further adding graphene into a polymer, the phenomenon of graphene restacking together occurs due to van der Waals force of the nanosheets. Then

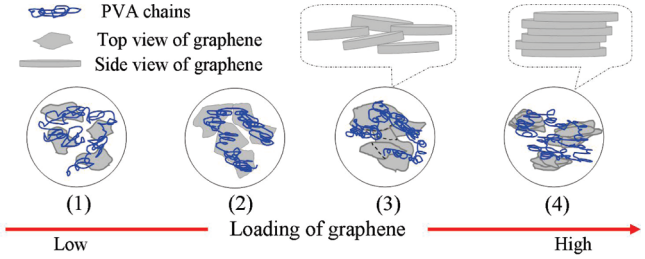

Figure 11. Schematic models of various dispersion types of graphene nanosheets in PVA matrix: (1) Graphene nanosheets are individually dispersed in the matrix at intervals. (2) The edges of graphene nanosheets just join together side by side. (3) Some of graphene nanosheets are overlapping with each other. (4) Graphene nanosheets are restacking together by layers. As increasing graphene content, the resulting dispersion form gradually changes.

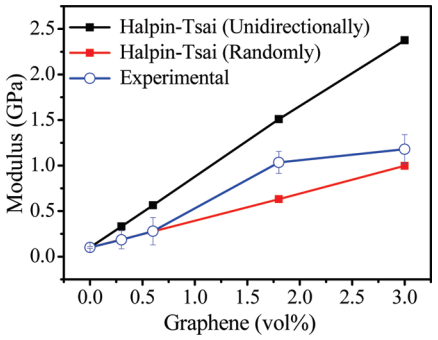

Figure 12. Young's moduli of the nanocomposite and Halpin−Tsai theoretical models. The theoretical simulations were taken as two cases: the random orientation and unidirectional distribution of graphene nanosheets in the polymer matrix.

the slippage of piled graphene nanosheets during the tensile testing will have less effective enhancement on the mechanical properties of the composite. This can be explained from the schematic models in Figure 11. It is assumed that there are four types of arrangements for the nanosheets in the polymer matrix upon increasing nanofillers: (1) they are individually dispersed in the matrix at intervals, (2) the edges of the sheets just join together side by side, (3) there are some parts of the flakes overlapping with each other, and (4) the graphene slices are stacking together by layers. Among these, the second one (2) is the ideal condition, exhibiting the ultimate contribution to the mechanical behaviors with the greatest efficiency. With the increase of graphene loading, the arrangement would be changed from (1) to (3). When the amount of fillers reaches a critical content and the distance between two sheets is so small that they may be apt to stack together easily due to the van der Waals force, then it turns to the restacked form (4). There exists a critical point of the mechanical properties upon the nanosheet content, i.e., a loading of 1.8 vol %, and this phenomenon is called as *mechanical percolation* in our laboratory, similar to electrical or rheological percolations.[40] Lower than this content, the exfoliated graphene nanosheets can be well-dispersed in the polymer matrix, and the increase of loading has a significant improvement on the mechanical properties, while further loading may cause the nanosheets stacking together, weakening the efficiency of the mechanical improvement.

The Young's moduli of the nanocomposites are shown in Figure 12 (with circles). The trend of the modulus with graphene loading is similar to that of tensile strength. Compared to pristine PVA/SDBS films, the modulus of the nanocomposite with 1.8 vol % graphene loading is more than 10 times greater (from 0.10 to 1.04 GPa). Therefore, the large

aspect radio of graphene nanosheets and strong interactions between the graphene and the PVA matrix greatly enhance the mechanical performance of the nanocomposites.

The Halpin−Tsai equation is a simple approximate form to predict the modulus of unidirectional or randomly distributed filler-reinforced composites.[41−43] To study the distribution of graphene nanosheets in the polymer matrix, the Halpin−Tsai equation was used to simulate the modulus of the graphene/PVA nanocomposites. Considering the random orientation or unidirectional distribution of graphene nanosheets in the polymer matrix, the modified Halpin−Tsai equation is written as follows:[44,45]

$$E_C = \left[\frac{3}{8}\frac{1 + (2L_G/3T_G)\eta_L V_G}{1-\eta_L V_G} + \frac{5}{8}\frac{1 + 2\eta_T V_G}{1-\eta_T V_G}\right]E_P \quad (1)$$

$$E_{Paral} = \left[\frac{1 + (2L_G/3T_G)\eta_L V_G}{1-\eta_L V_G}\right]E_P \quad (2)$$

$$\eta_L = \frac{(E_G/E_P) - 1}{E_G/E_P + 2L_G/3T_G} \quad (3)$$

$$\eta_T = \frac{(E_G/E_P) - 1}{E_G/E_P + 2} \quad (4)$$

where E_C and E_{Paral} are the Young's moduli of the composites with randomly oriented and unidirectionally distributed graphene nanosheets, and the latter refers to aligned parallel to the surface of the sample. E_P and E_G are the tensile modulus of PVA and graphene. L_G, T_G, and V_G represent the length, thickness, and volume fraction of graphene in the composite, respectively. The Young's modulus of the PVA parallel sample is 0.1 GPa from the experimental results, and that of free-standing monolayer graphene is ~1.0 TPa.[2] The thickness and average length of graphene nanosheets are 0.8 nm and 1 μm obtained from AFM and TEM images. Young's moduli of the composites with two supposed distributions of graphene nanosheets are calculated and compared with the experimental data in Figure 12. The figure shows the theoretical simulation for the random distribution of graphene nanosheets is consistent with the result of the experimental data. Apparently, the dispersion of graphene nanosheets in polymer matrix is mostly random, not aligned parallel to the surface of the composite films. Furthermore, there is a tiny distinction for the Young's modulus of 1.8 vol % loading, which can be attributed to our assumption of critical point that analyzed above.

4. Conclusions

The graphene-based PVA composite films with improved uniformity and good dispersion were successfully prepared by incorporating graphene oxide into PVA matrix and reducing graphene oxide into graphene nanosheets. The graphene/PVA composite films exhibited a significant improvement on the mechanical properties. As a representative example, a 150% increase of tensile strength were achieved by adding 1.8 vol % graphene nanosheets, indicating the efficient load transfer between the graphene nanosheets and the matrix. The modulus of the composite with 1.8 vol % graphene loading is more than 10 times greater than the parallel PVA sample. Upon the loading of the nanosheets, it is assumed that there might be a critical point of the extent of improvements to the mechanical properties. The comparison between the experimental results and the Halpin−Tsai theoretical prediction indicated that graphene nanosheets might be randomly dispersed in the polymer matrix. Moreover, the addition of graphene nanosheets into the PVA matrix had a slight effect on the crystallinity of the composites. Apparently, graphene/PVA nanocomposites were successfully prepared with significant improvement of mechanical properties in this report. However, more work should be continued. Dispersion of the bulk quantity graphene nanosheets and the easy incorporation of the nanofillers into a matrix and further improvement of mechanical properties via enhancing the interfacial interaction between the nanosheets and a polymer matrix or the alignment of the nanosheets in a matrix are the key challenges.

Acknowledgment. Financial support of this work is provided by NSFC (50873021, 50925312), Shuguang (09SG30), Program for New Century Excellent Talents in University (NCET-06-0421), Shanghai Leading Academic Discipline Project (B603), and the 111 Project (111-2-04 and B07024).

References and Notes

(1) Novoselov, K. S.; Geim, A. K.; Morozov, S. V.; Jiang, D.; Zhang, Y.; Dubonos, S. V.; Grigorieva, I. V.; Firsov, A. A. *Science* **2004**, *306*, 666.
(2) Lee, C.; Wei, X. D.; Kysar, J. W.; Hone, J. *Science* **2008**, *321*, 385.
(3) Gómez-Navarro, C.; Burghard, M.; Kern, K. *Nano Lett.* **2008**, *8*, 2045.
(4) Balandin, A. A.; Ghosh, S.; Bao, W. Z.; Calizo, I.; Teweldebrhan, D.; Miao, F.; Lau, C. N. *Nano Lett.* **2008**, *8*, 902.
(5) Bolotin, K. I.; Sikes, K. J.; Jiang, Z.; Klima, M.; Fudenberg, G.; Hone, J.; Kim, P. *Solid State Commun.* **2008**, *146*, 351.
(6) Stoller, M. D.; Park, S. J.; Zhu, Y. W.; An, J. H.; Ruoff, R. S. *Nano Lett.* **2008**, *8*, 3498.
(7) Zhang, Y. B.; Tan, Y. W.; Stormer, H. L.; Kim, P. *Nature* **2005**, *438*, 201.
(8) Wang, X.; Zhi, L. J.; Mullen, K. *Nano Lett.* **2008**, *8*, 323.
(9) Fowler, J. D.; Allen, M. J.; Tung, V. C.; Yang, Y.; Kaner, R. B.; Weiller, B. H. *ACS Nano* **2009**, *3*, 301.
(10) Wang, C. Y.; Li, D.; Too, C. O.; Wallace, G. G. *Chem. Mater.* **2009**, *21*, 2604.
(11) Wang, Y.; Shi, Z. Q.; Huang, Y.; Ma, Y. F.; Wang, C. Y.; Chen, M. M.; Chen, Y. S. *J. Phys. Chem. C* **2009**, *113*, 13103.
(12) Eda, G.; Chhowalla, M. *Nano Lett.* **2009**, *9*, 814.
(13) Vickery, J. L.; Patil, A. J.; Mann, S. *Adv. Mater.* **2009**, *21*, 2180.
(14) Zhang, Q. H.; Lippits, D. R.; Rastogi, S. *Macromolecules* **2006**, *39*, 658.
(15) Verdejo, R.; Barroso-Bujans, F.; Rodriguez-Perez, M. A.; de Saja, J. A.; Lopez-Manchado, M. A. *J. Mater. Chem.* **2008**, *18*, 2221.
(16) Watcharotone, S.; Dikin, D. A.; Stankovich, S.; Piner, R.; Jung, I.; Dommett, G. H. B.; Evmenenko, G.; Wu, S. E.; Chen, S. F.; Liu, C. P.; Nguyen, S. T.; Ruoff, R. S. *Nano Lett.* **2007**, *7*, 1888.
(17) Yu, A. P.; Ramesh, P.; Itkis, M. E.; Bekyarova, E.; Haddon, R. C. *J. Phys. Chem. C* **2007**, *111*, 7565.
(18) Wakabayashi, K.; Pierre, C.; Dikin, D. A.; Ruoff, R. S.; Ramanathan, T.; Brinson, L. C.; Torkelson, J. M. *Macromolecules* **2008**, *41*, 1905.
(19) Liang, J. J.; Huang, Y.; Zhang, L.; Wang, Y.; Ma, Y. F.; Guo, T. Y.; Chen, Y. S. *Adv. Funct. Mater.* **2009**, *19*, 2297.
(20) Wang, D. W.; Li, F.; Zhao, J. P.; Ren, W. C.; Chen, Z. G.; Tan, J.; Wu, Z. S.; Gentle, I.; Lu, G. Q.; Cheng, H. M. *ACS Nano* **2009**, *3*, 1745.
(21) Liu, N.; Luo, F.; Wu, H. X.; Liu, Y. H.; Zhang, C.; Chen, J. *Adv. Funct. Mater.* **2008**, *18*, 1518.
(22) Bai, H.; Xu, Y. X.; Zhao, L.; Li, C.; Shi, G. Q. *Chem. Commun.* **2009**, *13*, 1667.
(23) Park, S.; Ruoff, R. S. *Nat. Nanotechnol.* **2009**, *4*, 217.
(24) Stankovich, S.; Dikin, D. A.; Piner, R. D.; Kohlhaas, K. A.; Kleinhammes, A.; Jia, Y.; Wu, Y.; Nguyen, S. T.; Ruoff, R. S. *Carbon* **2007**, *45*, 1558.
(25) Li, D.; Muller, M. B.; Gilje, S.; Kaner, R. B.; Wallace, G. G. *Nat. Nanotechnol.* **2008**, *3*, 101.
(26) Stankovich, S.; Piner, R. D.; Nguyen, S. T.; Ruoff, R. S. *Carbon* **2006**, *44*, 3342.
(27) Stankovich, S.; Dikin, D. A.; Dommett, G. H. B.; Kohlhaas, K. M.; Zimney, E. J.; Stach, E. A.; Piner, R. D.; Nguyen, S. T.; Ruoff, R. S. *Nature* **2006**, *442*, 282.

(28) Stankovich, S.; Piner, R. D.; Chen, X. Q.; Wu, N. Q.; Nguyen, S. T.; Ruoff, R. S. *J. Mater. Chem.* **2006**, *16*, 155.
(29) Hummers, W. S.; Offeman, R. E. *J. Am. Chem. Soc.* **1958**, *80*, 1339.
(30) Paredes, J. I.; Villar-Rodil, S.; Martinez-Alonso, A.; Tascon, J. M. D. *Langmuir* **2008**, *24*, 10560.
(31) Tuinstra, F.; Koenig, J. L. *J. Chem. Phys.* **1970**, *53*, 1126.
(32) Chieu, T. C.; Dresselhaus, M. S. *Phys. Rev. B* **1982**, *26*, 5867.
(33) Alvarez, L.; Righi, A.; Guillard, T.; Rols, S.; Anglaret, E.; Laplaze, D.; Sauvajol, J. L. *Chem. Phys. Lett.* **2000**, *316*, 186.
(34) Gao, C.; Jin, Y. Z.; Kong, H.; Whitby, R. L. D.; Acquah, S. F. A.; Chen, G. Y.; Qian, H. H.; Hartschuh, A.; Silva, S. R. P.; Henley, S.; Fearon, P.; Kroto, H. W.; Walton, D. R. M. *J. Phys. Chem. B* **2005**, *109*, 11925.
(35) Paredes, J. I.; Villar-Rodil, S.; Solis-Fernandez, P.; Martinez-Alonso, A.; Tascon, J. M. D. *Langmuir* **2009**, *25*, 5957.
(36) Lerf, A.; Buchsteiner, A.; Pieper, J.; Schottl, S.; Dekany, I.; Szabo, T.; Boehm, H. P. *J. Phys. Chem. Solids* **2006**, *67*, 1106.
(37) Wang, S.; Zhang, Y.; Abidi, N.; Cabrales, L. *Langmuir* **2009**, *25*, 11078.
(38) Qian, X. F.; Yin, J.; Yang, Y. F.; Lu, Q. H.; Zhu, Z. K.; Lu, J. *J. Appl. Polym. Sci.* **2001**, *82*, 2744.
(39) Hong, P. D.; Chen, J. H.; Wu, H. L. *J. Appl. Polym. Sci.* **1998**, *69*, 2477.
(40) Zhang, Q. H.; Fang, F.; Zhao, X.; Li, Y. Z.; Zhu, M. F.; Chen, D. J. *J. Phys. Chem. B* **2008**, *112*, 12606.
(41) Halpin, J. C.; Kardos, J. L. *Polym. Eng. Sci.* **1976**, *16*, 344.
(42) Qian, D.; Dickey, E. C.; Andrews, R.; Rantell, T. *Appl. Phys. Lett.* **2000**, *76*, 2868.
(43) Cadek, M.; Coleman, J. N.; Barron, V.; Hedicke, K.; Blau, W. J. *Appl. Phys. Lett.* **2002**, *81*, 5123.
(44) Mallick, P. K. *Fiber-Reinforced Composites: Materials, Manufacturing, and Design*; Marcel Dekker: New York, 1993.
(45) Zhang, X. F.; Liu, T.; Sreekumar, T. V.; Kumar, S.; Moore, V. C.; Hauge, R. H.; Smalley, R. E. *Nano Lett.* **2003**, *3*, 1285.